Cable-Path Optimization Method for Industrial Robot Arms

Shintaro Iwamura[a,b], Yoshiki Mizukami[c], Takahiro Endo[d], Fumitoshi Matsuno[e]

[a] Software Development Dept. Controller Div.
Product Business Division H.Q.
Industrial Automation Company,
Omron Corporation,
Shimogyo-ku, Kyoto, Japan
[b] Department of Mechanical Engineering and Science,
Kyoto University,
Kyodai-katsura, Nishikyo-ku, Kyoto, Japan
shintaro.iwamura@omron.com

[c] Graduate School of Science and Engineering
Yamaguchi University
Ube, Yamaguchi, Japan
mizu@yamaguchi-u.ac.jp

[d] Department of Mechanical Engineering and Science,
Kyoto University,
Kyodai-katsura, Nishikyo-ku, Kyoto, Japan
endo@me.kyoto-u.ac.jp

[e] Department of Mechanical Engineering and Science,
Kyoto University,
Kyodai-katsura, Nishikyo-ku, Kyoto, Japan
matsuno@me.kyoto-u.ac.jp

Abstract

The production line engineer's task of designing the external path for cables feeding electricity, air, and other resources to robot arms is a labor-intensive one. As the motions of robot arms are complex, the manual task of designing their cable path is a time-consuming and continuous trial-and-error process. Herein, we propose an automatic optimization method for planning the cable paths for industrial robot arms. The proposed method applies current physics simulation techniques for reducing the person–hours involved in cable path design. Our method yields an optimal parameter vector (PV) that specifies the cable length and cable-guide configuration via filtering the candidate PV set through

a cable-geometry simulation based on the mass–spring model. The proposed method offers two key features: 1) Increased computational efficiency via an optimization procedure that separates the entire cable into the cable segments. In the proposed method, the entire cable is segmented at the positions of the cable guides into several separate cable segments, and the PVs of the cable segments that satisfy the constraints of collision, stretch, and curvature radius are filtered into the local optimal PV set. The global optimal PV is obtained by finding the combination of the local optimal PVs which have the same guide configuration between the adjacent cable segments and have minimal total length of the adjacent cable segments. 2) Robustness to external disturbances, such as fluctuation in the physical properties of the cables and the accuracy of manually attaching the cables. The PVs of the local optimal PV sets are required to satisfy the above constraints, even if the cable length changes in the predefined range, which ensures the robustness of the obtained cable path. To verify the validity of the proposed method, we obtain the global optimal PVs by applying the method to several pick-and-place motions of a six-axis vertical articulated robot arm in our simulations and implement the cable paths on an actual robot arm based on the obtained PVs. Our results indicate that the proposed method can aid line engineers to efficiently design the cable paths along robot arms.

Keywords: Industrial robot, Cable-path optimization, Cable geometry, Physics simulation, Experimental validation

1. Introduction

Industrial robot arms have conventionally been used in processes requiring hard manual labor (e.g., the automobile industry) to perform simple and repetitive operations. More recently, industrial robot arms have been developed for application to multiproduct manufacturing in the electrical, electronics, food, and chemical industries. For multiproduct manufacturing, end effectors and sensors are attached to the robot arms. These end effectors and sensors include air chucks to pick up and carry products, equipment to spray adhesive, and cameras for inspection. The air, electricity, adhesive, or other materials are fed to the end effectors externally through cables.

Generally, these cables are fixed to the links of the robot arm with hooking guides. If the cable path is incorrectly laid out, the cable may collide with the robot arm or peripheral objects as the robot arm moves. To avoid this problem, the cable geometry and the possibility of its collision with objects should be checked at every moment of the motion. In cases wherein the cable collides with the robot arm or other objects, the cable length or the guide configuration must be adjusted. This process is referred to as cable-path planning.

As robot-arm motions are complex, the currently manual task of cable-path planning requires a considerable number of person–hours to address trials and errors involving the following aspects: observing the cable motion, planning the cable path, fabricating guides, attaching the cable, and

verifying the state of the attached cable. It is not unusual for an expert in the field to take more than a week for path planning. Herein we propose an automatic cable-path optimization method to reduce the person–hours required for cable-path design. In our method, an optimal cable-path solution is automatically filtered from the candidate parameter sets. This solution specifies the cable length and the guide configuration through a cable-geometry simulation. The main aim of this study is the automatic optimization of the cable path on industrial robot arms to significantly reduce the person–hours involved in the path planning process.

For cable-path optimization, it is necessary to run physics simulations on the geometric deformation of the cable associated with the robot arm's joint angles. Physics simulations, which virtually represent gravitation and the collisions of objects based on the laws of physics, are leveraged not only for animation, but also for computer-aided engineering applications, such as advance verification of product design. Herein, we focus on cables, which are flexible elastics and cannot be represented by simple rigid models in physics simulations. Thus far, several researchers have studied cable-simulation techniques. The Cosserat theory [1] is a well-known basic theory of micropolar elasticity for cable representation. It defines the independent translational and rotational degrees of freedom for each cable element. Based on the Cosserat theory, Spillmann and Teschner [2] divided a cable into one-dimensional (1D) discrete elements along the centerline and established a model to define the position and orientation of each cable element. They calculated the continuous deformation energies for each element using finite-element methods. Moreover, the dynamic relative configurations between the elements were calculated via the numerical integration of the Lagrangian equations of motion. Meanwhile, Grégoire and Schömer [3] conducted physics simulations of cables in the following manner: they divided a cable into 1D discrete elements and defined the bending and torsional energies as constraints of the elements and, subsequently, calculated the states of equilibrium for which the energy of the entire cable became minimal. In their study, they adopted a generalized mass–spring model to address boundary conditions, such as fixed and free ends, which resulted in simple and low-cost geometry calculations.

Meanwhile, the representation of object deformation models based on the mass–spring model has been studied for computer animation since the 1980s. Baraff and Witkin [4] performed physics simulations of the clothing worn by animated characters. A simple displacement spring was used in their simulations, and torsions were not considered. In another study, Hergenröther and Dähne [5] divided a cable into rigid cylinder segments and connected them by ball joints. However, these ball joints could not replicate torsion. Loock and Schömer [6] divided a cable into rigid segments and joined them using the mass–spring model. Their model could represent the torsion of a cable via the use of torsion springs in addition to linear and bending springs between segments. In addition, their CAD-based model allowed the detection of both cable self-collision and collision with peripheral objects. Lv et al. [7] performed physics simulations of cable harnesses using linear springs for

stretching, bending springs for bending, and torsion springs for geometrical torsion and material twisting. They observed the geometry of the cable harness during the movement of fixing clips.

To build upon this work, the position-based dynamics (PBD) framework has been proposed to increase the simulation speed and stabilize cable-collision detection with rigid bodies [8]. PBD have been implemented in many physics simulation engines, such as PhysX [9], Havok [10], and Bullet [11] and have been applied to computer games, animation, and physics simulations of liquids and clothing [12]. PBD can also represent actual material characteristics [13]. In this context, Umetani et al. [14] represented a cable using particles and "ghost" particles based on the Cosserat theory in the PBD framework, wherein the ghost particles were used to discretize material frames on a cable. The ghost particles held in place the geometry of the cable along a bending direction and acted as bending and twisting resistance when a force was applied. Kugelstadt and Schömer [15] further developed the work of Umetani et al., performing physics simulations of cables considering torsion without ghost particles by directly solving the constraints between particles and orthonormal frames. Here, we note that jointly simulating the motions of a robot arm and the attached cable required high computational efficiency and stability. Therefore, in this study, we conducted physics simulations of cable geometry using the mass–spring model on PhysX [9], in which the bending and torsion are adjustable.

The path optimization of robot motion is very important in the industrial scenes and has been studied by many researchers. Lu et al. [16] represented collision-free and smooth joint motion planning for six-axis industrial robots using B-spline curves. Larsen and Kin [17] calculated robot paths using evolutionary algorithms for producing aircraft components using carbon-fiber-reinforced plastics. Cvitanic et al. [18] applied robot pose optimization for milling hard materials using static and dynamic stiffness models. Weller et al. [19] applied tool-path airtime optimization in material-extrusion additive manufacturing using hybrid mixed-integer linear programming (MILP) models. Malhan et al. [20] developed a multi-robot cell to automate the layup process of carbon-fiber prepreg. Although the above mentioned studies did not consider the cable geometry during the robot-arm motion, Kressin [21] and Carlson et al. [22] applied cable-geometry simulations to the path optimization of robot-arm motion and discussed the mitigation of cable-dress-pack wear. They proposed two approaches to address the problem. The first optimized the motion path to exclude problematic robot configurations as determined through a preliminary simulation and to prevent the robot joint from rotating with large angles that significantly stressed the dress pack. The second approach optimized the motion path without considering the dress pack and subsequently introduced the deformation and stress of the dress pack into the path optimization. The stress of the dress pack was defined as a cost function composed of impulses from peripheral objects, the stretch, and the curvature radius. Hermansson et al. [23] further developed on the study of Carlson et al. [22] and optimized robot paths with respect to quasi-static motions and deformations to overcome contact problems by introducing more inertia into the system. In the abovementioned approaches, optimized robot paths with fixed dress-pack

configurations were provided; however, the optimization of the dress-pack configuration itself was not discussed. As described here, there are interesting studies for applying cable-geometry simulation to the path optimization of robot-arm motion, but we could not find previous studies where the cable-geometry simulation is applied to the optimization of the cable path for a given robot-arm motion.

To address this deficiency, in this work we focused on cable-path optimization under the condition that the motion of the robot arm had already been determined. We optimized a parameter vector (PV) that included the cable length and cable-guide configuration. As the cable is generally attached to the robot-arm links by means of fixing guides, it is also necessary to optimize the cable lengths between guides. However, the number of parameters is too large for efficient optimization if the guide positions attaching the entire cable and the cable lengths between these guides are simultaneously optimized. Therefore, we regarded the entire cable as composed of optimized cable segments separated by adjacent guides. We set the following constraints: the impulse received by the cable in motion, the cable stretch, and cable curvature radius must not exceed certain thresholds. In addition, these constraints must be satisfied even if the cable was shortened or elongated within a certain range to ensure robustness against disturbances, such as errors in the physics simulation or length fluctuation of manually attached cables. Herein, we note that a global optimal PV for the entire cable cannot be obtained simply by combining local optimal PVs for each cable segment; adjacent cable segments must also share the configuration of a guide that connects the segments together. Therefore, the global optimal PV is obtained by finding the combination of the local optimal PVs which have the same guide configuration between the adjacent cable segments and have minimal total length of the adjacent cable segments. In the case of multiple global optimal PVs, we selected the solution for the shortest full-length cable.

The rest of this paper is organized as follows: the cable-path optimization is formulated in Section 2. In Section 3, optimal PVs acquired through simulation are examined. The proposed method is examined for its effectiveness using an actual robot arm in Section 4. Finally, Section 5 summarizes the study and discusses our future work.

2. Proposed Method

We propose an automatic method to optimize the path of the cable fixed to the links of a robot arm with cable guides. Given robot-arm motion requirements, the cable-guide configurations and cable lengths must be optimized to prevent collisions with peripheral objects and cable damage during long operational intervals.

Figure 1 shows an N-link robot arm. Cable guide $G_n(n = 1, \dots, N)$ is affixed to link $L_n(n = 1, \dots, N)$, and cable segment $C_n(n = 1, \dots, N)$ is connected to both G_n and G_{n+1}. We set coordinate system Σ_{L_0}, whose origin is the base of link L_0, as the absolute coordinate system. Coordinate system Σ_{L_n}, whose origin is the base of link L_n, is "overlaid" on L_n. The configuration

of link L_n at time t is represented as a nonlinear function of joint angle $\Theta(t) = [\theta_1(t), \theta_2(t), \dots, \theta_N(t)]^T$. The black dots P_n in Fig. 1 represent the device attachment points, and guide G_n is attached to the point of link L_n. The configuration of guide G_n with respect to Σ_{L_n} is given by the relative configuration based on the device attachment position P_n. The configuration of guide G_n in Σ_{L_0} is a function of joint angles $[\theta_1(t), \theta_2(t), \dots, \theta_n(t)]^T$ and P_n.

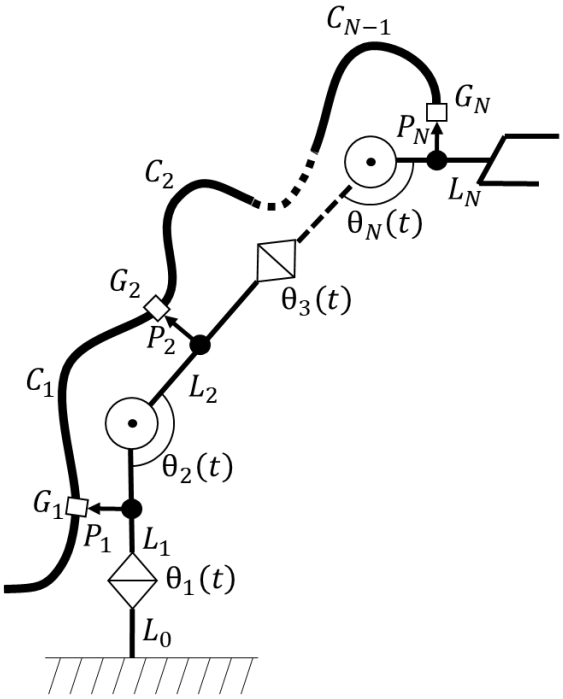

Fig. 1. Schematic of N-link robot arm considered in the study along with the cable and guide placement.

In our approach we employ a cable-geometry model based on multiple rigid sub-segments with a certain physical size and the virtual mass–spring joint [7, 9, 11,24] and conduct physics simulations. The virtual joint with six degrees of freedom (DoF) acts as a constraint for two adjacent sub-segments. According to Hooke's law, force (F_x, F_y, F_z) and torque $(\tau_\varphi, \tau_\theta, \tau_\psi)$ are proportional to the difference between the initial relative configuration and the current relative configuration of any two adjacent sub-segments. Thus, we have

$$\begin{bmatrix} F_x \\ F_y \\ F_z \\ \tau_\varphi \\ \tau_\theta \\ \tau_\psi \end{bmatrix} = \mathrm{diag}(\kappa_x, \kappa_y, \kappa_z, \kappa_\varphi, \kappa_\theta, \kappa_\psi) \begin{bmatrix} \tilde{x} - x \\ \tilde{y} - y \\ \tilde{z} - z \\ \tilde{\varphi} - \varphi \\ \tilde{\theta} - \theta \\ \tilde{\psi} - \psi \end{bmatrix} - \mathrm{diag}(\zeta_x, \zeta_y, \zeta_z, \zeta_\varphi, \zeta_\theta, \zeta_\psi) \begin{bmatrix} \dot{x} \\ \dot{y} \\ \dot{z} \\ \dot{\varphi} \\ \dot{\theta} \\ \dot{\psi} \end{bmatrix} \tag{1}$$

In the above expression, the first term on the right-hand side corresponds to the proportional term of Hooke's law; here, $\kappa_x, \kappa_y, \kappa_z, \kappa_\varphi, \kappa_\theta, \kappa_\psi$ denote the spring stiffnesses, (x, y, z) the current relative position, and (φ, θ, ψ) the current relative orientation of roll, pitch, and yaw angles. Furthermore,

$(\tilde{x}, \tilde{y}, \tilde{z}, \tilde{\varphi}, \tilde{\theta}, \tilde{\psi})$ together denote the initial relative configuration. The second term is the damping term; $\zeta_x, \zeta_y, \zeta_z, \zeta_\varphi, \zeta_\theta, \zeta_\psi$ represent damping coefficients and the dot operator above the current relative configuration represents its first derivation.

Cable segment C_n consists of S_n sub-segments and virtual joints, as illustrated in Fig. 2; that is, S_n denotes the number of sub-segments in C_n. Thus, the length of C_n, l_{c_n}, depends on S_n. The length of sub-segment is defined as l_{ss}, resulting in $l_{c_n} = S_n \times l_{ss}$. The first sub-segment of C_n is affixed to guide G_n, and the S_nth sub-segment is connected to the first sub-segment of cable segment, creating C_{n+1} via the S_nth virtual join. The geometry of cable segment C_n is obtained by calculating the configurations of the S_n sub-segments. As only adjacent sub-segments can connect to each other, the corresponding constraint equation is composed of sparse matrices. Therefore, the convergence solution can be derived using an iterative method, such as the Gauss–Seidel method. As the configurations of G_n and G_{n+1} with respect to Σ_{L_0} change over time, the geometry of C_n with respect to Σ_{L_0} also changes.

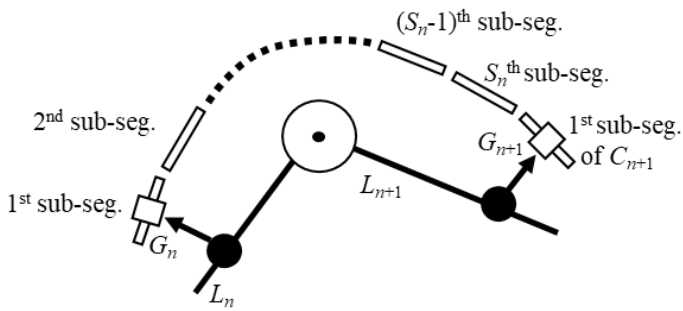

Fig. 2. Sub-segments contained in cable segment C_n.

Figure 3 shows the procedure of the cable-path optimization method, which consists of three main processes: joint-angle time-series generation, local optimization for each cable segment, and global optimization for the entire cable. Each step is described in the following sections: the joint-angle time-series $\Theta(t)$ is obtained from a list of transit poses (Section 2.1); the local optimal parameter vector (PV) set $D_{2,n}$ are obtained by satisfying several conditions for each cable segment (Section 2.2), and the global optimal PV, d^*, is obtained by finding the combination of the local optimal PVs which have the same guide configuration between the adjacent cable segments and have minimal total length of the adjacent cable segments. (Section 2.3)

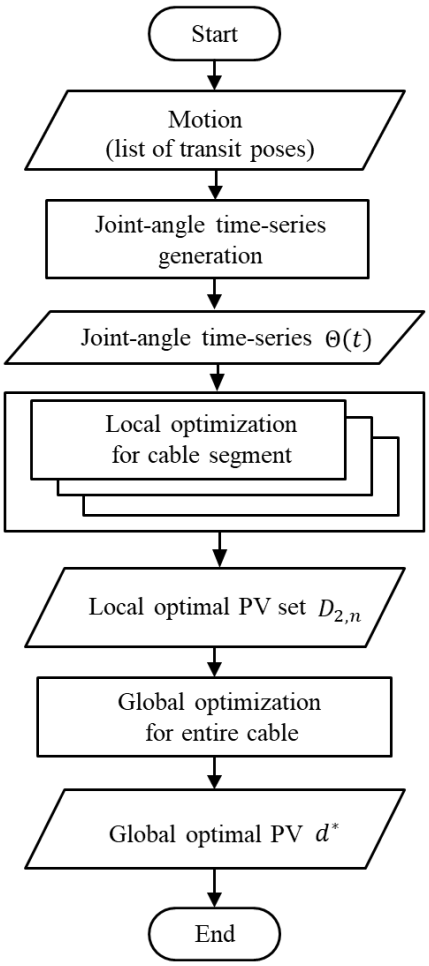

Fig. 3. Cable-path optimization procedure.

2.1. Joint-angle time-series generation

An operator determines the robot-arm motion based on a list of preset transit poses. This list of poses and their sequencing is called the joint-angle time-series. There are two main techniques for generating this series. The first is to specify the sequential poses of the robot arm in a virtual robot-simulating environment. The second technique is direct teaching, wherein the operator instructs the sequential poses of the physical robot arm by using a special controller, such as a robot teach pendant [25].

Planning a motion to execute all the transit poses in a list is a matter of optimization. It is required to satisfy the following constraints: reducing energy consumption, avoiding collisions, and meeting the limits of speed and torque. The joint-angle time-series $\Theta(t)$ is generated as a solution to this optimization problem.

2.2. Local optimization for a cable segment

Herein, we describe the local optimization for cable segment C_n. There are three candidate parameters that required optimization: S_n (the number of sub-segments in C_n), P_n (the

configuration of guide G_n), and P_{n+1} (the configuration of G_{n+1}). The candidate PV set is composed of all the combinations of the candidate parameters, and each candidate PV is verified in the following manner. We prepare a cable-geometry model based on the physical parameters and subsequently calculate an initial cable geometry corresponding to the robot-arm pose with initial joint angle $\Theta(0)$. Next, we run a physics simulation to calculate the cable geometry corresponding to the joint-angle time-series $\Theta(t)$. Subsequently, we extract an optimal PV set satisfying the following constraints:

Condition 1: The impulse received by the cable when contacting with the robot arm or peripheral objects is less than threshold $Impulse_{th}$.

Condition 2: The stretch rate of the distance between adjacent sub-segments on the cable to a predefined distance is less than threshold $Stretch_{th}$.

Condition 3: The minimum cable curvature radius is more than threshold $Curvature_{th}$ as determined by the cable material.

We define $D_{0,n}$ as a candidate PV set that is generated from all parameter combinations:

$$D_{0,n} = \{(S_{n,i_n}, P_{n,j_n}, P_{n+1,j_{n+1}}) | 1 \le i_n \le I_n, 1 \le j_n \le J_n, 1 \le j_{n+1} \le J_{n+1}\}, \tag{2}$$

where $\{S_{n,i_n} | 1 \le i_n \le I_n\}$ denotes the candidate set of the number of sub-segments contained in C_n that connect L_n and L_{n+1}, and I_n denotes the number of candidates for the sub-segments. The sub-segment numbers in the candidate set should be distributed at regular intervals of ΔS in a search range; therefore, we prepare S_{n,i_n} so as to be an arithmetic progression for i_n. Moreover, $\{P_{n,j_n} | 1 \le j_n \le J_n\}$ denotes the candidate set of configurations of G_n attached to L_n, and J_n is the number of candidates of the guide configuration. $\{P_{n+1,j_{n+1}} | 1 \le j_{n+1} \le J_{n+1}\}$ also denotes the candidate set of configurations of G_{n+1} attached to L_{n+1}. We define $D_{1,n}$ as a subset of $D_{0,n}$ that contains PVs satisfying the abovementioned three conditions.

$$\begin{aligned} D_{1,n} = \{(S_{n,i_n}, P_{n,j_n}, P_{n+1,j_{n+1}}) \in D_{0,n} | \\ Impulse_{th} > \max_{1 \le t \le T} Impulse_{(S_{n,i_n}, P_{n,j_n}, P_{n+1,j_{n+1}})}(t), \\ Stretch_{th} > \max_{1 \le t \le T} Stretch_{(S_{n,i_n}, P_{n,j_n}, P_{n+1,j_{n+1}})}(t), \\ Curvature_{th} \le \min_{1 \le t \le T} Curvature_{(S_{n,i_n}, P_{n,j_n}, P_{n+1,j_{n+1}})}(t)\}, \end{aligned} \tag{3}$$

where $Impulse_{(S_{n,i_n}, P_{n,j_n}, P_{n+1,j_{n+1}})}(t)$ expresses the maximum value of an impulse received by all sub-segments contained in C_n at time t. Similarly, $Stretch_{(S_{n,i_n}, P_{n,j_n}, P_{n+1,j_{n+1}})}(t)$ and $Curvature_{(S_{n,i_n}, P_{n,j_n}, P_{n+1,j_{n+1}})}(t)$ express the stretch rate and the curvature radius of the sub-segments contained in C_n, respectively. It is noteworthy that all PVs in $D_{1,n}$ cannot be applied to an actual robot arm as an optimal PV for C_n, because some of the PVs in $D_{1,n}$, when applied practically, can damage the cable owing to external disturbances, such as the length fluctuation of the manually attached cable. Other disturbances can arise from an estimation error of the spring stiffness of the cable and an approximation error in the physics simulation. In addition, we must notice that the physical properties of the cable are not necessarily homogeneous or isotropic due to being curled in the shipping packaging and the effects of the robot-arm motion. To overcome this problem, we examine the

robustness of the PVs in $D_{1,n}$, and we define $D_{2,n}$ as a subset of $D_{1,n}$ that includes only the PVs with a certain level of robustness. We focus on the robustness related to the length of C_n (the number of sub-segments) such that the PVs will satisfy the abovementioned three conditions even when the number of sub-segments increases or decreases within a predefined range parameter of robustness R. By referring to the segment-length fluctuation corresponding to the robustness as l_R, $R = l_R/(\Delta S \times l_{ss})$. Let us define a set of the R-neighbor PVs of $(S_{n,i_n}, P_{n,j_n}, P_{n+1,j_{n+1}})$ related to i_n, which is the index of S_{n,i_n}, as

$$D_{neighbor,(S_{n,i_n},P_{n,j_n},P_{n+1,j_{n+1}})} = \{(S_{n,i'_n}, P_{n,j_n}, P_{n+1,j_{n+1}}) | \\ i_n - R \le i'_n \le i_n + R, 1 \le i'_n \le I_n\}, \tag{4}$$

The local optimal PV set $D_{2,n}$ is expressed as follows:

$$D_{2,n} = \{(S_{n,i_n}, P_{n,j_n}, P_{n+1,j_{n+1}}) \,|\, D_{neighbor,(S_{n,i_n},P_{n,j_n},P_{n+1,j_{n+1}})} \subset D_{1,n}, \\ 1 \le i_n - R, i_n + R \le I_n\}, \tag{5}$$

where the second and third conditions for $D_{2,n}$ are introduced so as to ensure that $D_{neigbhor,(S_{n,i_n},P_{n,j_n},P_{n+1,j_{n+1}})}$ includes the PVs that are R apart from $(S_{n,i_n}, P_{n,j_n}, P_{n+1,j_{n+1}})$ in both sides along the index of S_{n,i_n}. Please note that $D_{2,n}$ may include a PV whose neighbor set does not have the width of $2R$ without these conditions.

2.3. Global optimization for the entire cable

We next discuss the estimation of a global optimal PV that minimizes the total number of sub-segments through the entire cable via combining the PVs contained in $\{D_{2,n} | 1 \le n \le N\}$ and obtained through local optimization of the cable segments $\{C_n | 1 \le n \le N\}$. First, we introduce the adjacency condition in which adjacent cables must share the configuration of the guide that tethers them. The PV set D_3, which satisfies the adjacency condition, can be expressed as

$$D_3 = \{S_{1,i_1}, \dots, S_{n,i_n}, \dots, S_{N-1,i_{N-1}}, P_{1,j_1}, \dots, P_{n,j_n}, \dots, P_{N,j_N} | \\ (S_{n,i_n}, P_{n,j_n}, P_{n+1,j_{n+1}}) \in D_{2,n}, 1 \le n < N\} \tag{6}$$

The PVs included in D_3 are referred to as applicable PVs. We note here that the applicable PVs satisfy all of the impulse, stretch rate, curvature radius, and adjacency conditions. Next, we define d^* as a global optimal PV that has the smallest total number of sub-segments through the entire cable, leading to finding the minimum total length of cable segments:

$$d^* = \arg\min_{d} \sum_{n=1}^{N-1} S_{n,i_n} \quad d \in D_3 \tag{7}$$

When there are multiple candidates of global optimal PVs with the same total number of sub-segments, one is selected as d^* by considering the priorities between impulse, stretch rate, and curvature radius.

3. Simulation

We applied the proposed cable-path optimization method to several different pick-and-place motions of a six-axis, vertical, articulated robot arm (Omron Viper 850 [26]). We employed Fujikura AWG28x5P IFVV-SB cable [27] attached to the robot arm. In the following sections, we first describe the parameterization of the guides and cables. Next, we describe the simulation procedures in the order illustrated in Fig. 3: that is, joint-angle time-series generation, local optimization for cable segments, and global optimization for the entire cable. We also analyze the obtained PVs from quantitative and qualitative viewpoints.

3.1. Parameterization of guides and cables on the robot arm

We defined the parameters related to the sub-segment numbers of the cable segments and guide configurations to be optimized. Figure 4 illustrates the labels of the guides and cables with those of the links. The origin of the absolute coordinate system Σ_{L_0} is fixed at the base of the robot arm. The origins of Σ_{L_3} and Σ_{L_4} are fixed at the bases of L_3 and L_4, respectively. An end effector is attached to L_6, and guide G_6 is substituted with a cable receptacle on the end effector. That is, configuration P_6 is predetermined according to the specification of the end effector. C_4 is tethered to G_4 and G_6 without passing through G_5, as it is impossible to attach a cable guide at L_5 owing to the robot-arm structure. In this configuration, the parameters related with C_4 to be optimized are the number of sub-segments S_4 and the guide configuration P_4. Moreover, C_3 is tethered to G_3 and G_4, and therefore S_3, P_3, and P_4 are added to the set of parameters to be optimized. We did not employ C_2 for tethering G_2 and G_3, as any cable from a rack or ceiling would be tethered to G_3. Consequently, we optimized the cable path composed of cable segments C_3 and C_4 with relaying G_3 and G_6 via G_4. As mentioned previously, P_5 and P_6 did not need to be optimized. Therefore, the final set of parameters to be optimized were S_3, S_4, P_3, and P_4.

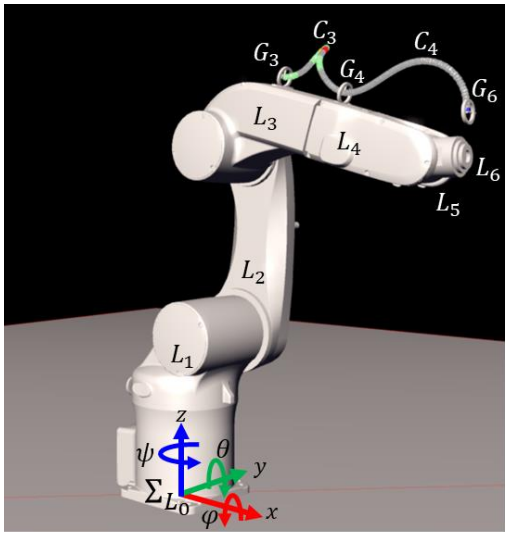

Fig. 4. Six-axis vertical articulated robot arm with the cable.

3.2. Joint-angle time-series generation

Pick-and-place motion is frequently used for industrial robot applications; therefore, we investigated the efficacy of the proposed method by applying it to seven pick-and-place motions. We defined the motion as a series of robot poses with respect to Σ_{L_0}: the robot arm picks an object in front along the x-axis at $(x, y, z) = (500\text{ mm}, 0\text{ mm}, 170\text{ mm})$ and then places it with a certain yaw angle α to the front-left at $(x, y, z) = (400\text{ mm}, 400\text{ mm}, 170\text{ mm})$. We considered seven different yaw angles for placing the object, α, ranging from $-90°$ to $45°$ in steps of $15°$ around the z-axis of Σ_{L_0} while the position, roll, and pitch angles of the object to be placed were fixed. Robot-arm motion with the place angle of α is expressed as *motion with* α in the following description. Figure 5 illustrates the snapshots of the poses including the pick pose and place poses with different yaw angles. All motions began with the initial pose shown in Fig. 5(a). Subsequently, the robot arm completed the pick pose shown in Fig. 5(b) and returned to the initial pose through one of the place poses. Figures 5 (c), (d), and (e) show the place poses for *motion with* $-45°, 0°,$ and $45°$, respectively. In the study, we used a robot programming environment, Omron ACE [28], to edit the motion programs and generate the joint-angle time-series $\Theta(t)$ corresponding to the seven pick-and-place motions.

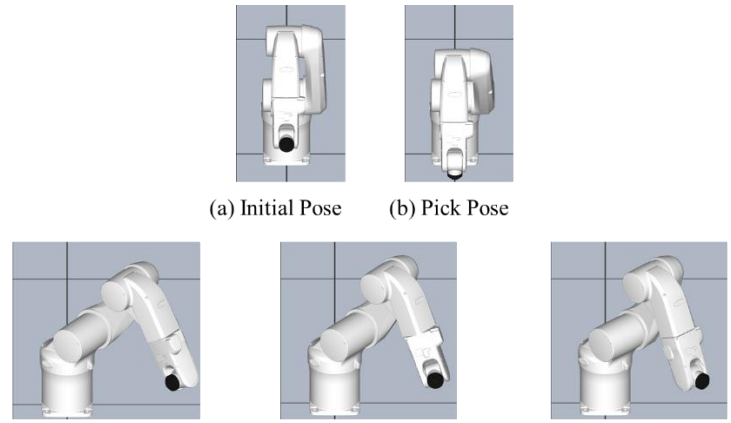

(a) Initial Pose (b) Pick Pose

(c) Place Pose (−45°) (d) Place Pose (0°) (e) Place Pose (45°)

Fig. 5. Poses in pick-and-place motions of the robot arm.

3.3. Local optimization for cable segments

To optimize the local path of cable segments C_3 and C_4, we defined the candidate parameters S_3, S_4, P_3, and P_4. Here, we explain the preparation of these candidate parameters.

We began with candidate parameters S_3 and S_4. The minimum values of S_3 were determined based on the distance between the device attachment points on L_3 and L_4 at the initial pose. Similarly, the minimum values of S_4 were determined based on the distance between the device attachment points on L_4 and L_6. The maximum values of S_3 and S_4 were determined by adding an adequate range value to the corresponding minimum values, where the range value was chosen with considering the existence of the solution and the computational time. Consequently, the cable-length of C_3 was set at a range of 100 mm to 300 mm, and the cable length of C_4 was set at 200 mm to 440 mm. We determined the length of a unit sub-segment as 5 mm, and the step width of the cable-segment length for optimization was set to 20 mm. Therefore, the candidates for S_3 and S_4 were $(S_{3,1}, S_{3,2}, \cdots, S_{3,11}) = (20, 24, \cdot\cdot, 60)$ and $(S_{4,1}, S_{4,2}, \cdots, S_{4,13}) = (40, 44, \cdot\cdot, 88)$, respectively. The numbers of candidates were $I_3 = 11$ and $I_4 = 13$ and the regular intervals of ΔS was set at 4. The unit sub-segment length of 5 mm was represented as a connection of a cylinder of length 3.5 mm with the diameter of 8 mm and a sub-segment interspace (virtual joint) of 1.5 mm. The range parameter of robustness, R, was set at $2(= \frac{l_R}{\Delta S \times l_{ss}} = \frac{40\text{mm}}{4\times 5\text{mm}})$ so as to tolerate 40 mm-length fluctuation, l_R, of C_3 and C_4.

As mentioned previously, position (x, y, z) and orientation (φ, θ, ψ) of P_n were defined based on the device attachment position at L_n in the coordinates of Σ_{L_n}. Hereafter, the units of position and orientation are millimeters and degrees, respectively. The φ direction is the twisting direction of the cable. In our study, φ was fixed to 0 because the life of the cable is shortened if the cable is attached

after being twisted. The position candidate set for P_3 was $\{(x,y,z)|x=0, y=-40,0,40, z=0,20\}$ and the orientation of P_3 was fixed to $(\varphi,\theta,\psi)=(0,0,0)$, leading to $J_3=6$. In contrast, the position candidate set for P_4 was $\{(x,y,z)|x=0,50, \mathrm{y}=-50,0,50, \mathrm{z}=0,20\}$ and the orientation candidate set of P_4 was $\{(\varphi,\theta,\psi)|\varphi=0, \theta=0,45, \psi=-90,0,90\}$, leading to $J_4=72$. As mentioned previously, $J_6=1$ because the configuration P_6 of G_6 was fixed. The parameter combinations of C_3 and C_4 were 4,752 and 936, respectively.

Next, we describe the procedure to obtain the optimal PVs for C_3 and C_4. $Impulse_{th}$ in Eq. 3 was set to 0 so as to remove PVs which led to collisions with peripheral objects. $Stretch_{th}$ was set at 102%. Although $Stretch_{th}$ has a natural limit of 100% from the viewpoint of the physical stress, it was set at 102% for this procedure in order to tolerate the oscillation of the solutions during preliminary simulations. $Curvature_{th}$ was set at $48\,\mathrm{mm}$ as six times of the cable diameter as specified in the cable specification. With regard to C_3, we conducted physics simulations on all the PVs included in PV set $D_{0,3}$ and obtained PV set $D_{1,3}$, which satisfied the three conditions. Subsequently, we derived the optimal PV set $D_{2,3}$ considering the robustness. Similarly, with regard to C_4, we determined $D_{1,4}$ and $D_{2,4}$ based on $D_{0,4}$.

The values of spring stiffness and damping coefficient in Eq. 1 were estimated using the procedure described in the Appendix. It took approximately ten hours to optimize the C_3 parameters and two hours for the C_4 parameters. We employed the mass–spring model in PhysX SDK 4.0 to perform the physics simulations of the cable geometry, wherein rigid segments were connected with six DoF virtual joints. The specifications of the computer used for the simulations were as follows: Windows 10 Professional OS, Intel Core i9-7980XE 2.6 GHz CPU, 16 GB RAM, and NVIDIA GeForce RTX 2080 GPU.

3.4. Global optimization for the entire cable

We first generated the applicable PVs D_3 satisfying the adjacency condition between cable segments C_3 and C_4 from the optimal PV sets $D_{2,3}$ and $D_{2,4}$. Next, we calculated the global optimal PV set d^* for the entire cable.

Here, we provide a quantitative analysis regarding the difficulty of planning the cable path for a given motion of the robot arm based on the obtained set D_3. Figure 6 shows the number of PVs in D_3 obtained for different motions. At *motion with* $45°$, wherein the angle difference between L_3 and L_4 for the place pose was 0°, we obtained 71 applicable PVs. However, the number of applicable PVs decreased as the place angle decreased. At *motion with* $-60°$, only one applicable PV was obtained. There was no applicable PV at *motion with* $-75°$, which indicated that no cable path was available for the robot-arm motion and implied the need to redesign the production line from several viewpoints, including robot-arm motions, the angles at which the target item was placed, and the positions of the

peripheral objects.

Next, we qualitatively analyzed the geometry of the cable path for the given motion of the robot arm based on the global optimal PV d^*. Figure 7 shows d^* of the entire cable for *motion with* $45°, 0°,$ and $-45°$ and the cable geometries at the pick and place poses. At a *motion with* $45°$, the angle difference between L_3 and L_4 is $0°$. Therefore, two symmetrical optimal PVs exist, i.e., right-to-left and left-to-right cable geometry. However, when the place angle decreases (*motion with* $0°$ and $-45°$), the joint between L_3 and L_4 turns counterclockwise, and the cable arrangement is configured as left-to-right cable geometry. As the rotation angle formed by L_3 and L_4 for the place pose of *motion with* $-45°$ is larger than the rotation angle at *motion with* $0°$, the cable may collide with the upper-edge of L_4. Therefore, the position of G_4 $(0, -50, 20)$ at *motion with* $-45°$ moves to the upper-right when compared with G_4 position $(50, 0, 20)$ at *motion with* $0°$. These results show that the guide position was optimized as so to avoid collision with the robot arm. To satisfy the condition of the minimum curvature radius at the place pose, the cable length of C_4 at *motion with* $-45°$ was extended by 60 mm when compared to the corresponding length at *motion with* $0°$. Despite this extension, the entire-cable length when compared with that at *motion with* $0°$ was extended by only 20 mm $((44 + 72) - (52 + 60)) \times 5)$ because the cable length of C_3 at *motion with* $-45°$ was shorter by 40 mm $((52 - 44) \times 5)$ when compared with that of *motion with* $0°$.

We note here that the abovementioned quantitative and qualitative analyses can be applied to other robot-arm motions or robot-arm architectures and can aid line engineers in accomplishing any robot movement task.

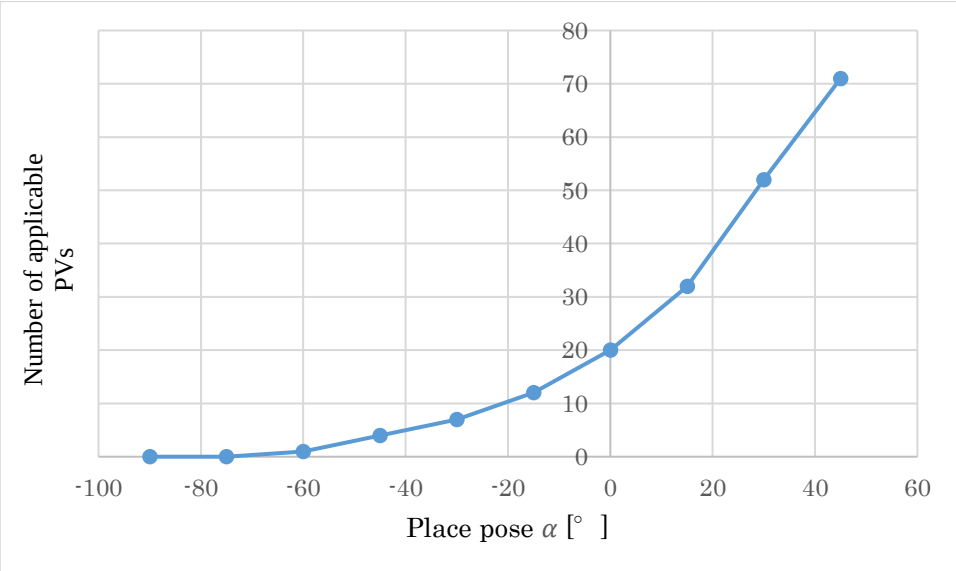

Fig. 6. Arm motion and the corresponding number of optimal PVs.

Motion angle	45°		0°	-45°
d* (S_3, S_4, P_3, P_4)	Right-to-left cable geometry	Left-to-right cable geometry	Left-to-right cable geometry	Left-to-right cable geometry
	(48,60, (0,40, 0,0, 0,0), (50,0,0,0, 0, -90))	(48,60, (0,-40,0, 0,0, 0), (50,0, 0,0, 0,90))	(52,60, (0,-40,0,0,0,0) (50,0,20,0,0,90))	(44,72, (0,-40,0,0,0,0), (0,-50,20,0,0,90))
Pick	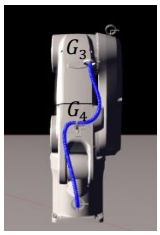	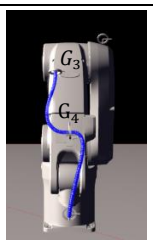	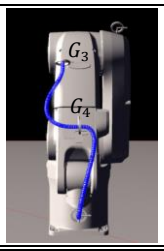	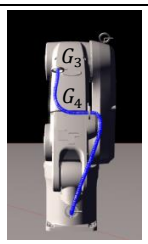
Place				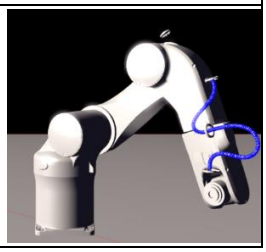

Fig. 7. Global optimal PVs d^* for different robot-arm motions and cable geometries for the pick and place poses.

4. Experimental validation

4.1. Setup procedure

To evaluate the validity of the global optimal PV d^* and the accuracy of the cable-geometry simulation, the cable path was implemented on an actual robot arm. We employed d^* obtained at *motion with* $-45°$, as mentioned in Section 3. The reason we focused on *motion with* $-45°$ was that this motion was one of the most complex among the proposed motions. The rotation angle of link L_4 in relation to L_3 was large, and the possibility of cable collision with the robot was high. The specification of the cable was the same as that employed in the simulation: Fujikura AWG28x5P IFVV-SB. According to the sub-segment numbers of the cable segments and the guide configurations of d^*, we attached the cables of corresponding lengths on the robot arm with guides of the corresponding configurations.

4.2. Experimental results

Figure 8 illustrates the cable geometries for the pick and place poses in the simulation and actual experiment. Figures 8(a) and (b) show the simulation results, whereas Figs. 8(c) and (d) show the

corresponding experimental results with the actual robot arm. The cable geometries obtained in the experiment were nearly identical to the counterpart ones in the simulations. We also visually confirmed in supplementary video 1 that, through the robot-arm motion, the cable neither contacted the robot arm nor extended beyond the specified range. Moreover, we measured the curvature radius at the place pose in the experiment; this radius was smallest through the motion in the simulation. The experimental curvature radius was 53 mm and larger than the threshold value of $Curvature_{th}$= 48 mm.

Next, to evaluate the accuracy of the cable-geometry simulation, we measured the actual cable geometry as point cloud data using a 3D scanner (PhoXi 3D Scanner S [29]). Figure 9 shows the robot arm attached with the cable and the 3D scanner. We fastened white tape at the middle and 50 mm-distance positions on cable segments C_3 and C_4, and we specified the middle-position tapes as markers. These markers can easily be identified in Figs. 8(c) and (d). Using the coordinate system Σ_{L_0}, we examined the differences between the coordinates of these markers and those of the corresponding cable sub-segments in the simulation. As it was impossible to measure the coordinates of a moving object owing to the 3D-scanner limitations, we measured the marker coordinates on the robot arm while paused at three poses: pick, halfway (an intermediate pose between pick and place), and place poses. Figure 10 shows the overlaid images of the cable geometry and the point cloud data for these three poses; the point cloud data corresponding to the markers on C_3 and C_4 (marker point clouds) are indicated in red, whereas the other point clouds are in green. Additionally, the blue and light blue circles indicate the coordinates of the centers of gravity of the marker point clouds and the middle sub-segments of the cable segments, respectively. The coordinates of the centers of gravity of the marker point clouds and the middle sub-segments on C_3 and C_4, and the corresponding differences, are listed in Table 1. The maximum differences for C_3 and C_4 were 17.6 mm and 21.6 mm, respectively. We assume that the causes of these differences were estimation errors of the spring stiffness, the cable attachment error along the φ direction, and the weakly curled shape of the cable owing to its looped bundling in the shipping package. The obtained difference was not significantly large, which confirms that the simulation based on the mass–spring model adopted in this study is reliable for cable-path planning.

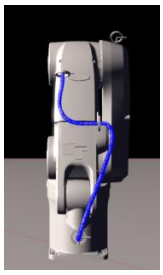

(a) Pick Pose (Simulation)

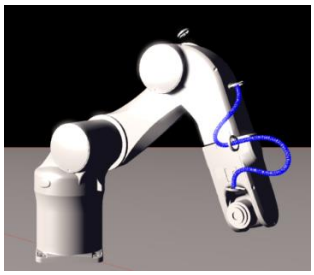

(b) Place Pose (Simulation)

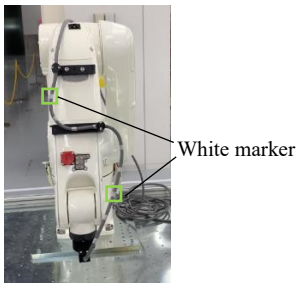

(c) Pick Pose (Experiment)

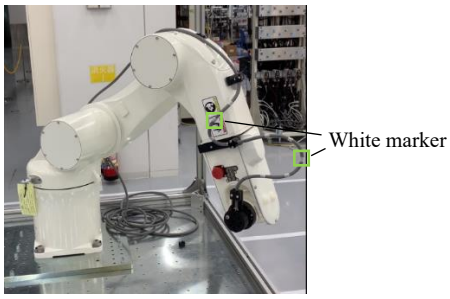

(d) Place Pose (Experiment)

Fig. 8. Simulated and experimental results for *motion with* $-45°$, where $d^* = (S_3, S_4, P_3, P_4) = (44,72,(0,-40,0,0,0,0),(0,-50,20,0,0,90))$.

Fig. 9. Measurement of point cloud data with a 3D scanner.

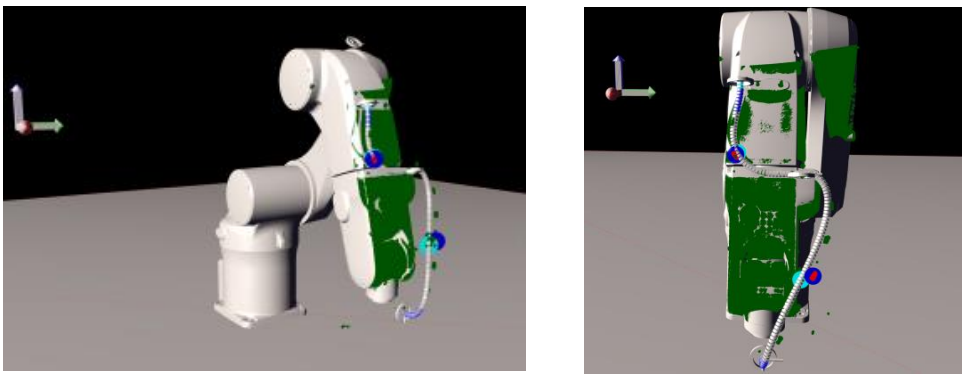

(a) Pick pose

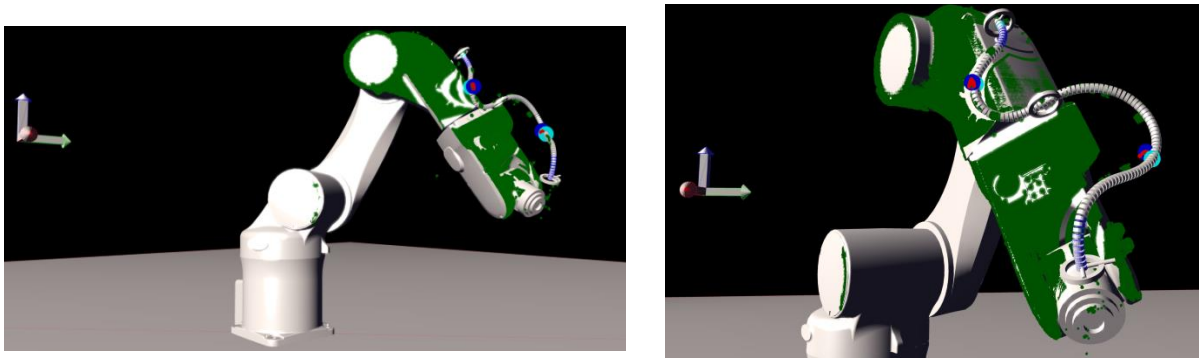

(b) Halfway pose (Intermediate pose between pick and place)

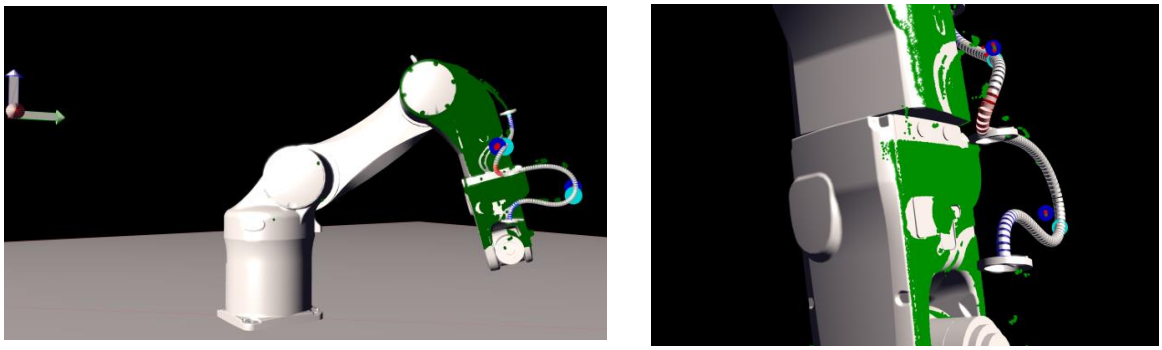

(c) Place pose

Fig. 10. Overlaid images of the point cloud data measured by the 3D scanner and the simulation results.

Table 1. Coordinate differences at marker positions between simulation and experiment.

	C_3 Middle cable segment						
	The corresponding sub-segments in simulation [mm]			Gravity centers of marker point cloud [mm]			Difference [mm]
	x	*y*	*z*	*x*	*y*	*z*	
Pick	519.4	-43.9	462.5	524.3	-46.3	460.3	5.8
Halfway	451.7	165.5	567.6	462.4	161.2	566.6	11.6
Place	405	380.6	402	398.5	364.2	402.3	17.6

	C_4 Middle cable segment						
	The corresponding sub-segments in simulation [mm]			Gravity centers of marker point cloud [mm]			Difference [mm]
	x	*y*	*z*	*x*	*y*	*z*	
Pick	577.8	51.8	290.1	580.9	68.4	297.3	18.4
Halfway	525.7	341.7	476.8	518.7	338.3	484.3	10.8
Place	499.1	498	292.7	490.7	508.2	309.8	21.6

5. Discussion

5.1. Effectiveness of robustness

In order to clarify the effectiveness of robustness introduced in this study, we applied the optimal PVs with and without robustness to the actual robot with *motion with* $-45°$. As defined in Section 3.2, *motion with* -45° means the robot-arm motion with the place yaw angle of -45°. Let us refer to these two conditions as Case wR ($R = 2$ in Eq. 4 and 5) and woR ($R = 0$), respectively. Figure 11 illustrates the shape of C_3 and C_4 in each case. According to Fig. 11(a) and (b), C_3 did not contact the corner of the robot arm in Case wR with a segment length of 220 mm, but it did in Case woR with a length of 180 mm. According to Fig. 11(c) and (d), the curvature radius of C_4 in Case wR with a length of 360 mm was 53 mm, which was over the threshold radius of 48 mm, but the radius in Case woR with the length of 320 mm was 46 mm, which violated the threshold radius. These observations indicate that the robustness was effective for planning reliable cable paths on actual robot arms.

(a) wR (with robustness) in C_3 (b) woR (without robustness) in C_3

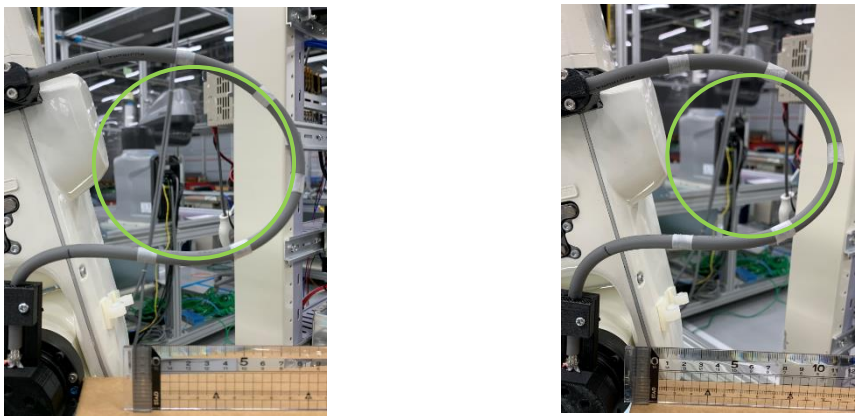

(c) wR (with robustness) in C_4 (d) woR (without robustness) in C_4

Fig. 11 Experimental result of the optimal PVs with and without robustness.

5.2. Computational efficiency of cable-segment simulation

The proposed method increased the computational efficiency by performing the cable-geometry simulation after separating the entire cable into cable segments at the adjacent guides. In order to confirm the computational efficiency of the proposed method, we compared the computation time of the entire-cable simulation with that of the cable-segments one. The PC used in the simulation of Section 3 was reused.

The number of parameter combinations in the entire-cable simulation was 46,332: the simulation time was approximately 201 hours. As reported in Section 3.4 in the cable-segment simulation of the proposed method, the parameter combinations of C_3 and C_4 were 4,752 and 936, respectively, and the total simulation time was approximately 12 hours. The simulation time for the cable-segment simulation was less than a tenth of that of the entire-cable simulation due to the reduced combination parameters. These results indicate the computational efficiency was significantly increased by separating the entire cable into the cable segments.

5.3. Cable path planning by an inexperienced engineer

In order to emphasize the usefulness of the proposed method, we report on the designed cable paths and the engineer's comments obtained when an inexperienced engineer was engaged to design the cable path for the robot-arm motion employed in Section 4.

Although the engineer had qualifications for operating industrial robots based on Article 59 of the Industrial Safety and Health Act in Japan [30], he lacked experience in cable path design. G_3 and G_4 guide attachments were fabricated with a 3D printer so as to change the guide configurations, and an end-effector attachment was also fabricated with a 3D printer.

We asked the engineer to design a cable path for the pick-and-place *motion with* $-45°$. Before the work, we explained the three constraints by showing the notes and presented the robot-arm motion until he was satisfied. We had him adjust the position of the guides and the cable length so that the overall cable length would be shortened. As the work of changing the guide position and cable length requires skill, another engineer partially assisted in the changeover work.

He designed the cable path 12 times. Figure 12 shows the initial, intermediate, and final paths, as well as the path obtained using the proposed method (same as Fig. 8). The entire cable length finally obtained was 660 mm (C_3 230 mm and C_4 430 mm), which was 80 mm longer than the entire cable length obtained by the proposed method. After approximately 2.5 hours, the engineers abandoned further improvement and finished the design work. During the work, the end-effector was seriously damaged due to an undersized cable length, and we had to replace it with a spare one.

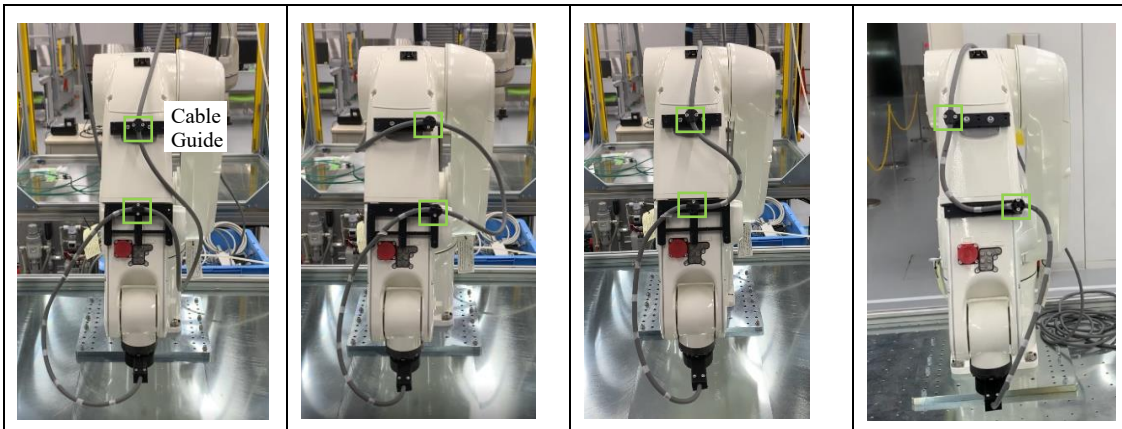

Initial	Intermediate	Final	Proposed method

Fig. 12. Cable path design by an engineer.

The comments given by the inexperienced engineer were as follows:

- *I tried to optimize the cable path by repeating the process of checking the cable deformation through the actual robot motion and then making modifications, but when optimized to a certain degree, I could not figure out how to make further modifications. Lastly, I sometimes designed the paths inferior to the previously designed ones.*

- *I had physical fatigue through repeating the cable attaching work, since I had to change the guide configuration and the cable length so as not to hit my head on the safety frame around the robot arm. I felt that I wanted to minimize the number of trial-and-error steps as much as possible.*
- *In practical scenes, the end-effectors and cables are expensive. If an engineer does not have enough experience, the engineer might break them by carelessness.*

Through cable path planning by an inexperienced engineer, the following observations were acquired.

- Cable path planning using the proposed method gave a shorter cable length than that designed manually by an engineer.
- The proposed method reduced the mental and physical load on the engineer.
- The proposed method avoided damage to the equipment due to the use of inappropriate cable length.

The obtained observations and the inexperienced engineer's comments indicate that the proposed method is useful for engineers to reduce their burden for planning cable paths on the robot arm and avoiding damages on the cable and equipment by a carelessly designed cable path.

6. Conclusion

In this study, we proposed an automatic optimization method for planning the cable path on industrial robot arms. Our method outputs a global optimal PV specifying the cable length and cable-guide configuration by filtering the candidate PV set obtained via cable-geometry simulations based on the mass–spring model. The proposed method has two beneficial features: increased computational efficiency via an optimization procedure that separates the entire cable into cable segments and robustness to external disturbances, such as fluctuations in the physical properties of the cables and the length of manually attached cables. The proposed method consists of three steps: joint-angle time-series generation, local optimization for cable segments, and global optimization for the entire cable.

In our simulations, we applied the proposed method to several different pick-and-place motions of a six-axis vertical articulated robot arm. We considered seven arm motions with different place angles and generated the joint-angle time-series for each of them. Our results demonstrated that the method could quantitatively determine the difficulty of planning the cable path for the given robot-arm motion based on the number of applicable PVs. In addition, the method can be used to qualitatively analyze the variation in the optimal cable paths associated with multiple motions based on the global optimal PV.

In our experiments, we applied the global optimal PV obtained in the simulations to an actual robot arm to evaluate the efficacy of the global optimal PV and the accuracy of the cable-geometry simulation. We applied the cable path according to the guide configurations and cable lengths of the global optimal PV and executed the pick-and-place motions with the robot arm. It was visually

confirmed that the global optimal PV satisfied the constraints related to collision with peripheral objects and cable stretch. Additionally, by measuring the minimum cable curvature radius, we confirmed that the constraint related to the curvature radius was satisfied. Moreover, to confirm the accuracy of the cable-geometry simulation, we scanned the point cloud data of the markers at the middle positions of the cable segments and compared the marker positions with the middle-segment positions obtained in the cable-geometry simulation for the pick, halfway, and place poses.

In our discussion, we clarified the effectiveness of the robustness by observing the actual cable geometries, the increased computational efficiency by comparing the computational time with and without separating the entire cable into cable segments, and the usefulness of the proposed method by reporting an inexperienced engineer's path-planning work.

In future, we plan to first focus on the curled shape of the cable. Here, although we used an electrical signal cable that was not tightly curled, hard cables (e.g., air cables) are shaped into loops for packaging. In such cases, the curled cable shape must be reflected in the derivation of the relevant physics parameters and the initial geometry of the simulations. Secondly, we plan to evaluate the person–hour reduction effect of the proposed method in many industrial scenes by comparing the work time of engineers for designing robot-arm cable paths with and without the proposed method.

[Appendix]

To estimate the spring stiffness required for the cable-geometry simulation, we employed a method similar to Scan2Flex [31]. In the method, we estimated the bending spring stiffness of virtual joint κ_θ based on the changes in the cable geometry due to gravity. However, κ_ψ was assumed to be equal to κ_θ owing to the cable structure. Considering the materials of a standard electrical signal cable, we set the values of $\kappa_x, \kappa_y, \kappa_z$ as 1.0×10^7 N/m so that the cable length did not change unless the cable collided with the robot arm or was stretched between the cable guides.

As shown in Fig. 13(a), we fixed one end of the cable horizontally and subsequently altered the cable length by 20 mm within the range of 100 to 200 mm and measured the vertical displacement of the ends of the cable. Table 2 lists the measured vertical displacement for each cable length. We constructed a cable model with the same length in our simulation and subsequently fixed one end horizontally, as shown in Fig. 13(b). The mass of the cable sub-segments was determined such that the total mass of all the sub-segments balanced the mass of the entire cable. A vertical acceleration of 9.8 m/s^2 was adopted as the force of gravity. Bending spring stiffnesses κ_θ for vertical displacement in each cable length are listed in the last row of Table 2. We repeated the following procedure to obtain κ_θ: after measuring the vertical displacement of an actual cable with one of the predefined lengths, the cable simulation was repeated while changing the values of κ_θ until the difference between the actual and simulated vertical displacement reduced to zero. Based on the average measured spring

stiffnesses, we determined κ_ψ (and κ_θ) as 7.1×10^{-2} N m/rad.

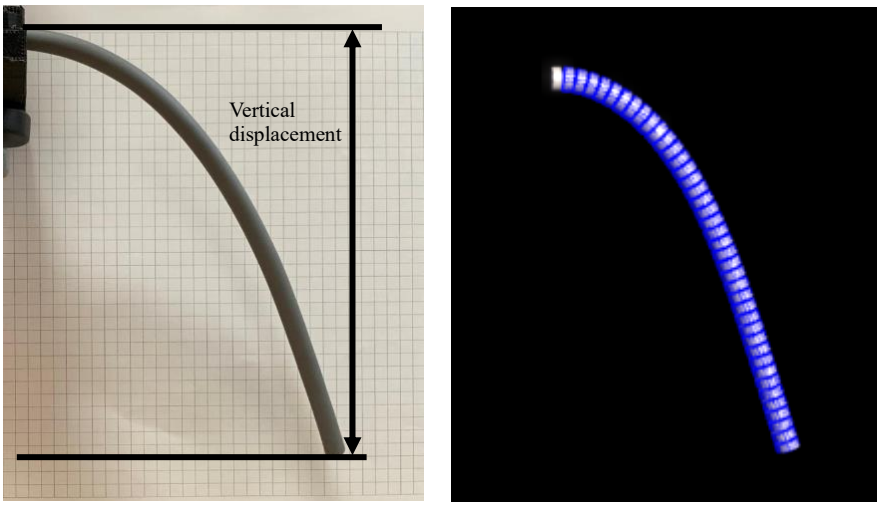

(a) actual cable used in the experiment (b) simulated cable

Fig. 13. Bending spring stiffness measurement.

Table 2. Relationship between vertical displacement and bending spring stiffness for cable lengths.

Cable length [mm]	100	120	140	160	180	200
Vertical displacement [mm]	30	45	60	90	120	140
Bending spring stiffness κ_θ[Nm/rad]	6.7×10^{-2}	7.3×10^{-2}	7.9×10^{-2}	7.1×10^{-2}	6.4×10^{-2}	6.9×10^{-2}

Secondly, we estimated the torsional spring stiffness of the virtual joint, κ_φ, according to the relationship between the angle of twist and the torsional moment of the cable. As illustrated in Fig. 14, torsional moment M is proportional to angle of twist φ as follows:

$$M = \kappa_\varphi \varphi \tag{7}$$

As shown in Fig. 15, one end of the 300 mm cable ($L = 300$) was fixed to a torque gauge (RZ-T-20, Aikoh Engineering [32]) and the other was fixed to the tip of the robot arm (Viper 850, Omron). The relationship between torsional moment M and angle of twist φ induced by the robot arm is plotted in Fig. 16. We calculated the gradient using the least-squares method and obtained a gradient of 2.57×10^{-2} N m/rad. This value was equivalent to the torsional spring stiffness of the entire cable, κ'_φ. In the simulation, the sub-segment unit length was set at 5 mm, corresponding to a total sub-segment number of 60, and the number of virtual joints, N, connecting these sub-segments was 60, resulting in $\kappa_\varphi = 1.5$ N m/rad according to $\kappa'_\varphi = \kappa_\varphi / N$.

We employed the damping coefficients $\zeta_x, \zeta_y, \zeta_z = 5 \times 10^2$ N s/m and $\zeta_\varphi, \zeta_\theta, \zeta_\psi = 5 \times 10^{-2}$ N m s/rad in Eq. 1 via trial and error in order to smooth out oscillations [33]. The analytical derivation of the damping coefficient will be discussed in a future work.

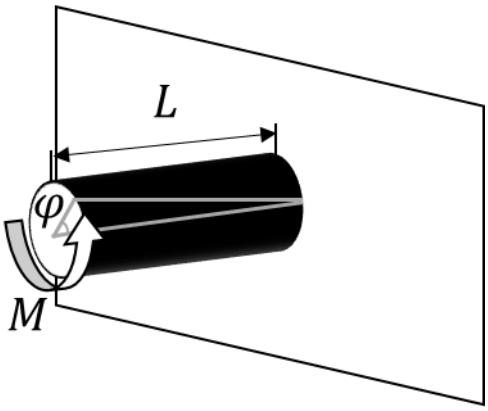

Fig. 14. Torsional moment M and angle of twist φ with respect to the cable centerline.

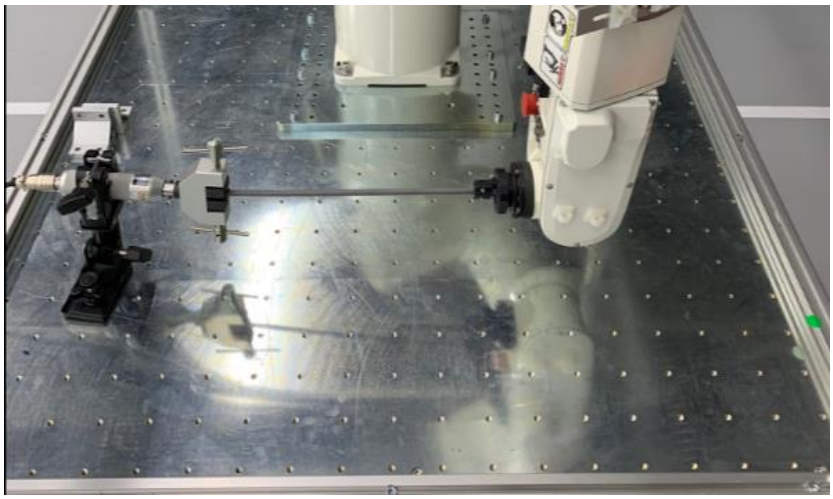

Fig. 15. Torsional moment measurement.

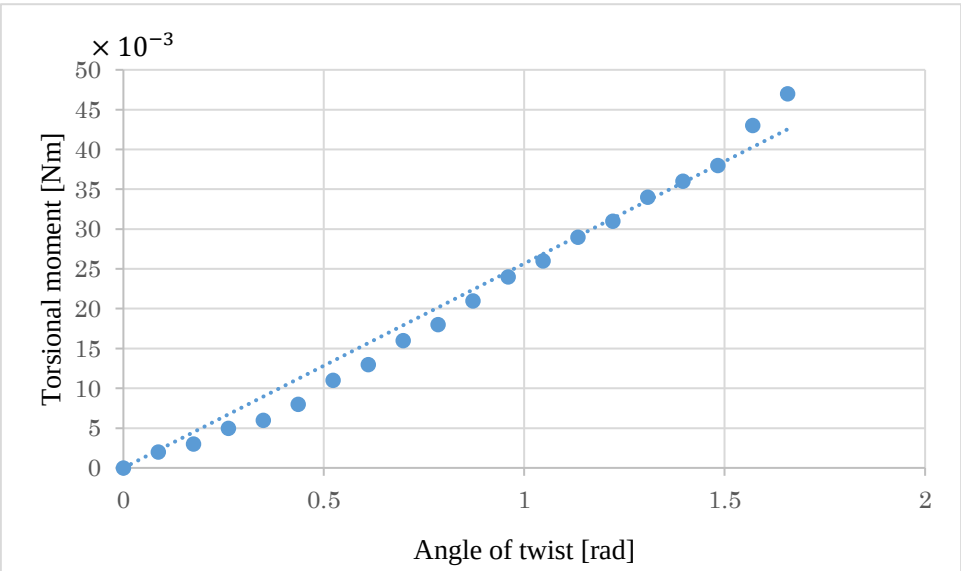

Fig. 16. Relationship between angle of twist φ and torsional moment.

Funding sources: This research did not receive any specific grant from funding agencies in the public, commercial, or not-for-profit sectors.

REFERENCES

[1] S.S. Antman, Nonlinear problems of elasticity, Appl. Math. Sci. 107 (2005). https://doi.org/10.1007/978-1-4757-4147-6_1.

[2] J. Spillmann, M. Teschner, CORDE: Cosserat rod elements for the dynamic simulation of one-dimensional elastic objects, Symp. Comput. Animat. 2007 - ACM SIGGRAPH/Eurographics Symp. Proceedings, SCA 2007, (2007) 63–72.

[3] M. Grégoire, E. Schömer, Interactive simulation of one-dimensional flexible parts, CAD Comput. Aided Des. 39 (2007) 694–707. https://doi.org/10.1016/j.cad.2007.05.005.

[4] D. Baraff, A. Witkin, Large steps in cloth simulation, Proc. 25th Annu. Conf. Comput. Graph. Interact. Tech. SIGGRAPH 1998, (1998) 43–54. https://doi.org/10.1145/280814.280821.

[5] E. Hergenröther, P. Dähne, Real-time virtual cables based on kinematic simulation, 8th International Conference in Central Europe on Computer Graphics, Visualization and Interactive Digital Media. Conference Proceedings Vol. 2 Pilsen: University of West Bohemia, 2000 (2000) 402–409.

[6] A. Loock, E. Schömer, A virtual environment for interactive assembly simulation: From rigid bodies to deformable cables, World Multiconference Syst. Cybern. Informatics (2001) 325–332. http://citeseerx.ist.psu.edu/viewdoc/download?doi=10.1.1.167.4262&rep=rep1&type=pdf.

[7] N. Lv, J. Liu, X. Ding, J. Liu, H. Lin, J. Ma, Physically based real-time interactive assembly simulation of cable harness, J. Manuf. Syst. 43 (2017) 385–399. https://doi.org/10.1016/j.jmsy.2017.02.001.

[8] M. Müller, B. Heidelberger, M. Hennix, J. Ratcliff, Position based dynamics, J. Vis. Commun. Image Represent. 18 (2007) 109–118. https://doi.org/10.1016/j.jvcir.2007.01.005.

[9] PhysX SDK, https://developer.nvidia.com/physx-sdk, 2021 (accessed 1 January 2021).

[10] Havok Physics, https://www.havok.com/havok-physics/, 2021 (accessed 1 January 2021).

[11] Bullet Real-Time Physics Simulation, (n.d.). https://pybullet.org/wordpress/, 2021 (accessed 1 January 2021).

[12] M. Macklin, M. Müller, N. Chentanez, T.-Y. Kim, Unified particle physics for real-time applications, ACMTOG 33 (2014) 1–12.

[13] J. Bender, M. Muller, M.A. Otaudy, M. Teschner, Position-based methods for the simulation of solid objects in computer graphics, ACM Trans. Graph. 27 (2013) 1. https://doi.org/ 10.2312/conf/EG2013/stars/001-022.

[14] N. Umetani, R. Schmidt, J. Stam, Position-based elastic rods, SCA 2014 - Proc. ACM SIGGRAPH/Eurographics Symp. Comput. Animat. (2014) 21–30.

[15] T. Kugelstadt, E. Schömer, Position and orientation based Cosserat rods, Symp. Comput. Animat. July 11 (2016) 169–178. https://doi.org/10.2312/sca.20161234.

[16] Y.A. Lu, K. Tang, C.Y. Wang, Collision-free and smooth joint motion planning for six-axis industrial robots by redundancy optimization, Robot. Comput. Integr. Manuf. 68 (2021) 102091. https://doi.org/10.1016/j.rcim.2020.102091.

[17] L. Larsen, J. Kim, Path planning of cooperating industrial robots using evolutionary algorithms, Robot. Comput. Integr. Manuf. 67 (2021) 102053. https://doi.org/10.1016/j.rcim.2020.102053.

[18] T. Cvitanic, V. Nguyen, S.N. Melkote, Pose optimization in robotic machining using static and dynamic stiffness models, Robot. Comput. Integr. Manuf. 66 (2020) 101992. https://doi.org/10.1016/j.rcim.2020.101992.

[19] T.R. Weller, D.R. Weller, L.C. de A. Rodrigues, N. Volpato, A framework for tool-path airtime optimization in material extrusion additive manufacturing, Robot. Comput. Integr. Manuf. 67 (2021) 101999. https://doi.org/10.1016/j.rcim.2020.101999.

[20] R.K. Malhan, A. V. Shembekar, A.M. Kabir, P.M. Bhatt, B. Shah, S. Zanio, S. Nutt, S.K. Gupta, Automated planning for robotic layup of composite prepreg, Robot. Comput. Integr. Manuf. 67 (2021) 102020. https://doi.org/10.1016/j.rcim.2020.102020.

[21] J. Kressin, Path optimization for multi-robot station minimizing dresspack wear, Master thesis, Chalmers University of Technology Department of Signals and Systems (2013).

[22] J.S. Carlson, J. Kressin, T. Hermansson, R. Bohlin, M. Sundbäck, H. Hansson, Robot station optimization for minimizing dress pack problems, Procedia CIRP. 44 (2016) 389–394. https://doi.org/10.1016/j.procir.2016.01.022.

[23] T. Hermansson, J.S. Carlson, J. Linn, J. Kressin, Quasi-static path optimization for industrial robots with dress packs, Robot. Comput. Integr. Manuf. 68 (2021) 102055. https://doi.org/10.1016/j.rcim.2020.102055.

[24] B. Yuan, H. Du, H. Wang, W. Xiong, The simulation of cable harness based on mass-spring model, MATEC Web Conf. 31 (2015) 1–4. https://doi.org/10.1051/matecconf/20153110002.

[25] C. Park, J.H. Kyung, H.M. Do, T. Choi, Development of direct teaching robot system, URAI 2011 - 2011 8th Int. Conf. Ubiquitous Robot. Ambient Intell. (2011) 730–732. https://doi.org/10.1109/URAI.2011.6145921.

[26] Omron Viper 850, http://www.ia.omron.com/products/family/3520/download/catalog.html, 2021 (accessed 1 May 2021).

[27] Fujilura Cable, https://www.fujikura-dia.co.jp/products/product04.php, 2021 (accessed 1 May 2021).

[28] Omron Automation Control Environment User's Guide, https://assets.omron.com/m/1b5d6fae43bfd7e6/original/ACE-User-s-Guide.pdf, 2021 (accessed 1 January 2021).

[29] Photoneo 3D Scanner, https://www.photoneo.com/phoxi-3d-scanner/, 2021 (accessed 1 May 2021).

[30] Industrial Safety and Health Act, https://www.jaish.gr.jp/anzen/hor/hombun/hor1-2/hor1-2-1-1h4-0.htm, 2021 (accessed 1 May 2021).

[31] T. Hermansson, S. Vajedi, T. Forsberg, F. Ekstedt, J. Kressin, C. Toft, J.S. Carlson, Identification of material parameters of complex cables from scanned 3D shapes, Procedia CIRP. 43 (2016) 280–285. https://doi.org/10.1016/J.PROCIR.2016.02.009.

[32] Aikoh Engineering Portable Torque Gauge, https://www.aikoh.co.jp/en/forcegauge/rzt/, 2021 (accessed 1 May 2021).

[33] Physx Joint User's Guide, https://docs.nvidia.com/gameworks/content/gameworkslibrary/physx/guide/Manual/Joints.html, 2021 (accessed 1 May 2021).